Polym. Bull. (2009) 63:755–771
DOI 10.1007/s00289-009-0151-y

ORIGINAL PAPER

Deformation behavior of isotactic polypropylene crystallized via a mesophase

Qamer Zia · Hans-Joachim Radusch · René Androsch

Received: 8 April 2009 / Revised: 20 August 2009 / Accepted: 21 August 2009 /
Published online: 30 August 2009

Abstract The mechanical behavior of semicrystalline isotactic polypropylene (iPP) of different crystallinity, crystal morphology and superstructure was investigated by standard tensile stress–strain analysis, dynamic-mechanical analysis, and in situ observation of the deformation by atomic force microscopy (AFM). Emphasis is put on the comparison of the mechanical characteristics of specimens containing either non-isometric lamellae, being arranged in spherulites, or nodular isometric domains, which are not organized in a superstructure. The formation of lamellae/spherulites and of nodules was controlled by the conditions of crystallization. The replacement of cross-hatched monoclinic lamellae and a spherulitic superstructure by randomly arranged isometric nodules leads to a distinct increase of the ductility and toughness, even if the crystallinity is identical. The modulus of elasticity and the yield stress increase as expected with increasing crystallinity. Slightly lower values of Young's modulus and yield strength are detected if samples contained non-lamellar crystals in a non-spherulitic superstructure, proving an effect of the crystal shape on the deformation behavior. For the first time, tensile deformation of semicrystalline iPP which contains nodular ordered domains instead of lamellae has been followed by in situ AFM.

Keywords Isotactic polypropylene · Crystal morphology · Superstructure · Deformation behavior · In situ atomic force microscopy

Q. Zia · H.-J. Radusch · R. Androsch (✉)
Center of Engineering Sciences, Martin-Luther-University Halle-Wittenberg,
06099 Halle/Saale, Germany
e-mail: rene.androsch@iw.uni-halle.de

Introduction

Isotactic polypropylene is a semicrystalline thermoplastic polymer of enormous and still increasing commercial importance due to favored combinations of ultimate properties which can be achieved at relatively low costs. These include mechanical properties which among others lead to applications in the field of classical engineering/construction, or optical properties which are important for film or packaging applications. Many properties are enhanced by modification of the neat polymer such as mechanical strengthening by incorporation of glass fibers, or optical clarification by addition of nucleation agents [1]. While high level of the modulus of elasticity and strength at temperatures higher than the glass transition temperature relies on the presence of the crystalline phase [2], light scattering on structural entities like spherulites, which typically form as a result of crystallization, is often connected with a loss of transparency [3]. As such, it seems a priori difficult to obtain an inherently transparent and simultaneously mechanically strong polymer.

In a recent study, we have demonstrated that optically transparent but highly crystalline films of iPP can be prepared by non-spherulitic crystallization, without employing optical clarifiers [4]. The required pathway of crystallization is shown in the left part of Fig. 1, that is, preparation of transparent semicrystalline non-spherulitic films of iPP includes in a first step rapid cooling and mesophase formation at ambient temperature, and then in a second step tailoring of the crystallinity, crystal structure and crystal size by annealing at elevated temperature, to control the mechanical characteristics. In detail, rapid cooling yields formation of randomly arranged, non-lamellar mesomorphic domains which on heating transform to monoclinic crystals of nearly identical habit, without affecting the absence of higher-order organization in a superstructure [5, 6]. Further details about the polymorphism and mesophase structure [7, 8], the morphology of the mesophase [9, 10], the kinetics/condition of mesophase formation [11, 12], the mesomorphic–monoclinic phase transformation [13, 14], or the evolution of the crystallinity on annealing [15] are reported elsewhere. The right part of Fig. 1 shows for comparison the path of crystallization on conventional melt-crystallization which typically leads to formation of lamellae and spherulites, and with that to optical non-transparency. It is emphasized that crystal size and crystallinity can be fine-tuned by the temperature and time of annealing in case of crystallization via the mesophase, and by the temperature of crystallization and subsequent annealing in case of conventional crystallization.

In the present study, we attempt to evaluate and compare the mechanical behavior of samples of iPP which were prepared according the pathways of crystallization presented in Fig. 1. Ultimately, we intend to show that non-spherulitic crystallization of iPP via the mesophase yields an advantageous combination of optical and mechanical properties which usually is not achieved without the use of additional aids like nucleating agents. Note that observation of a non-spherulitic superstructure and with that of transparent films can also be achieved by random copolymerization, which, however, is connected with distinct loss of crystallinity and mechanical strength. From this point-of-view, crystallization of iPP via the mesophase may offer additional options to tailor properties.

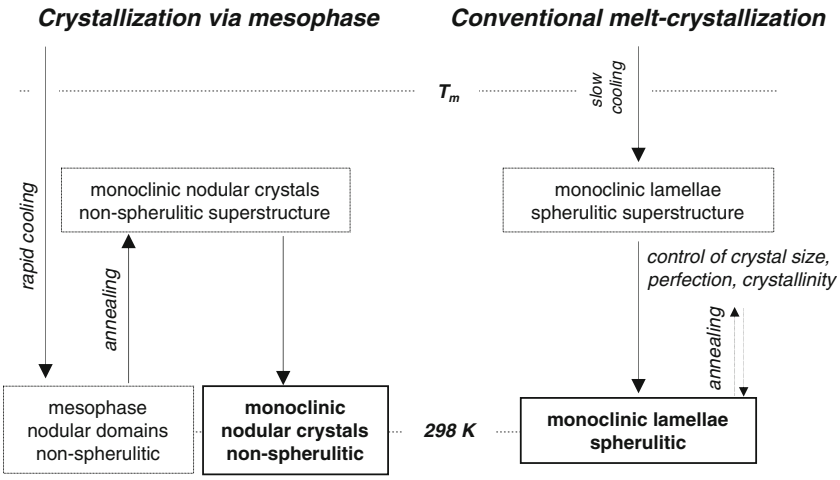

Fig. 1 Pathways of crystallization of iPP. Crystallization via the mesophase (*left*) results in formation of nodular crystals and a non-spherulitic superstructure while conventional melt-crystallization (*right*) leads to formation of lamellae and spherulites. The crystallinity can be adjusted identical

The deformation behavior of iPP, crystallized by conventional melt-crystallization, as was illustrated in the right part of Fig. 1, has extensively been studied in the literature. In general, in case of semicrystalline polymers containing lamellae within spherulites, tensile loading at temperatures higher than the glass transition temperature leads to deformation of amorphous chain segments, separation and rotation of lamellae, inter-lamellar shear, disintegration of spherulites, and fragmentation/dissolution of lamellae by fine and coarse slip [16–18]. The latter processes only occur if the local stress exceeds a critical value which is related to the macroscopically measured yield stress. In other words, deformation beyond the yield point mainly is by viscous flow of amorphous chain segments, and plastic deformation/slip of crystals, eventually leading to a structure of aligned micro-fibrils. In the specific case of iPP, even at temperatures above the glass transition temperature, however, frequently rather brittle failure is observed [19, 20]. Absence of plastic crystal deformation and fibrillation has been attributed to restricted mobility of amorphous chain segments which are interlocked in regions between cross-hatched lamellar α-crystals, which is a typical morphological feature of conventionally crystallized iPP [19, 21]. This conclusion was derived, e.g., from direct observation of the deformation process by scanning electron microscopy, and the comparison with iPP of higher ductility containing non-cross-hatched lamellar β-crystals/spherulites [19, 22, 23].

Investigation of the tensile stress–strain behavior of mesomorphic iPP revealed a distinctly higher deformability/ductility in comparison to conventionally crystallized samples [24–26]. The modulus of elasticity and the yield strength are lower, however, can be increased by subsequent annealing at elevated temperature, on expense of ductility. It was suggested that a major reason for the increase of the modulus of elasticity and yield strength on annealing is the increase of crystallinity [26, 27]. Despite annealing of initially quenched samples leads to a crystallinity

which is comparable to that of conventionally crystallized iPP, it is not connected with a total loss of ductility and a transition to brittle behavior. As such it is evidenced that the deformation behavior of iPP is controlled beside the crystallinity by additional parameters, such as the crystal morphology or the spherulitic superstructure [28, 29]. To date, an unequivocal discussion of the effect of spherulite size on the deformation behavior has not yet been achieved [28, 29], and the influence of the crystal morphology was not explored at all, neither in the specific case of iPP or other semicrystalline polymers.

As far as we are aware, there exist no comparative studies of the deformation behavior of iPP, performed on a single set of specimens crystallized according the different pathways of crystallization shown in Fig. 1. We prepared therefore a set of samples of such qualitatively different structures to establish a direct relation between the condition of crystallization, mechanical performance and optical transparency. For direct observation of deformation-induced changes of structure we applied in situ atomic force microscopy (AFM) which has not been applied yet to study the deformation of mesomorphic/monoclinic non-spherulitic iPP containing nodules, rather was only employed for monitoring the deformation of iPP containing lamellar crystals [30], or analysis of the structure of oriented films [31].

Experimental

Material

We used a commercial grade isotactic polypropylene from Montell Polyolefins with a mass-average molar mass and polydispersity of 373 kg mol^{-1} and 6.2, respectively. Samples of different structure were prepared by cooling films of 100 μm thickness at different rate between 10^{-1} and 10^{3} K s^{-1} from 473 K to ambient temperature, using a special device described in the literature [32], and subsequent annealing at different temperature. It has been shown in previous studies, that rapid cooling of films of 100 μm thickness at rates higher than 10^{2} K s^{-1} suppresses the formation of monoclinic lamellae and of spherulites, and results in formation of mesomorphic nodules at about ambient temperature, randomly distributed in an amorphous matrix [4–6, 11, 33]. In Fig. 1, this preparation step was denoted by '*rapid cooling*'. Subsequent annealing, denoted as '*annealing*' in Fig. 1, was performed at 393, 413, and 433 K in vacuum atmosphere, for a period of 60 min. Annealing led to the mesomorphic–monoclinic phase transformation, and growth of nodules from initially 15–20 nm up to 40 nm, depending on the annealing temperature. Conventional crystallization, leading to formation of monoclinic lamellae and spherulites was achieved by slow cooling at rates lower than 10^{2} K s^{-1}. Variation of the cooling rate between 10^{-1} and 10^{2} K s^{-1} affected the temperature of crystallization and with that the crystallinity, thickness of lamellae, and size of spherulites. The structure of these slowly cooled samples, furthermore, was also fine-tuned by subsequent annealing. Note that preparation of films of larger thickness than 100 μm may lead to structural heterogeneity across the film section [32], that is, all deformation experiments have been performed on 100 μm thin films.

Instrumentation

Tensile testing

The tensile stress–strain behavior was recorded on a miniature tensile testing machine MiniMat 200 from Rheometric Scientific, with a crosshead distance of 8 mm. In order to ensure deformation of the specimen at a pre-defined location, two semi-circular notches were introduced at half gauge length, imitating a shouldered test bar. The cross section of the films at the position of the notches was 0.1×2.2 mm^2. The strain rate during the initial test period of 10 s, for determination of modulus of elasticity, was 1 mm min^{-1}. Subsequently, the strain rate was increased to 10 mm min^{-1}. Modulus data were calculated manually, carefully considering useless data during the starting period of the test. Data reported are averages of five tests.

Dynamic-mechanical analysis (DMA)

Additional measurements of the modulus of elasticity were done in threshold-tensile mode using a DMA Mark III measuring head from Rheometric Scientific. The cross section and gauge length of the samples were 0.1×5 mm^2 and 8 mm, respectively. Samples were subjected to sinusoidal oscillating strain for a period of 5 min at ambient temperature. The pre-defined constant strain amplitude and frequency were 0.1% and 1 Hz, respectively. Measurements were performed at least two times, for calculation of an average value.

In situ atomic force microscopy (AFM) deformation

The initial morphology of the preparations at the nanometer scale was analyzed by a Quesant Q-scope 250 AFM, equipped with a 40 μm × 40 μm scanner. A standard silicon cantilever NSC 16 with a resonant frequency and force constant of about 170 kHz and 40 N m^{-1}, respectively, was used for image acquisition in height-mode contrast at ambient temperature. For deformation experiments, a home-made stretching device, fitting the AFM scanner/sample compartment, was used. The sample geometry was identical as in macroscopic tensile testing experiments. Images were recorded at constant, stepwise increasing strain, that is, loading/deformation of the samples was discontinuous. The local strain at the position of the AFM tip was estimated using the AMF camera and check marks at the sample surface with an initial distance at zero strain of 0.2 mm. Samples were allowed to relax for a period of about three minutes after each deformation step before collection of the image.

Results and initial discussion

Tensile stress–strain behavior

Figure 2 shows tensile stress–strain curves of iPP samples, which initially were solidified by continuous cooling from 473 K to ambient temperature at rates of 0.1

and 750 K s^{-1}, before and after annealing at elevated temperature. These samples were selected from a larger set of preparations as representatives of the crystallization regimes shown in Fig. 1. Slow cooling represents conventional crystallization, and rapid cooling is required for crystallization via the mesophase. The sample which was solidified at a rate of 0.1 K s^{-1} contains cross-hatched monoclinic lamellae of a thickness of 10–15 nm and spherulites of size of about 50–100 μm. The density-based crystallinity, that is, mass fraction of monoclinic crystals, is close to 50%. Tensile deformation of this preparation confirms the expected brittle behavior with the strain at break being of the order of only 10%. A post-yield deformation region is not detected for this particular specimen, that is, plastic crystal deformation and fibrillation is not observed. In contrast, the sample which was solidified at a rate of 750 K s^{-1}, containing mesomorphic nodules in a non-spherulitic superstructure, shows a rather ductile deformation behavior. The density of this preparation is lower than the density of slowly cooled specimens, which, however, is due to a lowered bulk density of the mesophase. Calculation of the mass fraction of mesophase revealed a value of 42%, that is, the mass fractions of the ordered phase in slowly and rapidly cooled iPP are approximately identical. Despite similar amount of the ordered phase, the tensile stress–strain behaviors are distinctly different.

Annealing of the slowly cooled sample leads to an increase of the yield strength as a function of the annealing temperature, without affecting the overall brittle deformation characteristics. Similarly, annealing of the initially rapidly cooled specimen is also connected with an increase of the yield strength; however, it is paralleled by a loss of ductility. Note that the tensile stress–strain curves of initially rapidly cooled and annealed iPP are shown only partly in Fig. 2, and that the decrease of the ductility due to annealing needs to be read from the provided values of the strain at break. Annealing, in both cases, initially slowly and rapidly cooled iPP, resulted in a maximum increase of the crystallinity to 64%, independent of the

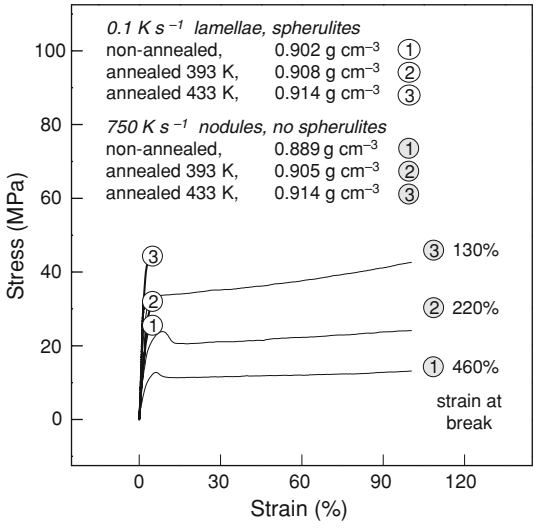

Fig. 2 Tensile stress–strain curves of iPP initially melt-crystallized at 0.1 and 750 K s^{-1}, and subsequently annealed at 393 and 433 K

prior cooling history. The deformation behavior after annealing, however, remained qualitatively different, that is, brittle behavior in case of the slowly cooled sample, and ductile behavior in case of the rapidly cooled iPP, in spite identical mass fraction of monoclinic crystals. Note that annealing of the rapidly cooled specimen allowed a transformation of the mesomorphic arrangement of molecule segments within the nodules into monoclinic structure. Since crystal structures and crystallinity are identical after annealing of the samples of a different initial cooling history, the different deformation behaviors can then only be explained by different crystal morphology and/or different superstructure.

Modulus of elasticity and yield stress

Figure 3 shows the modulus of elasticity (bottom) and yield strength (top) of iPP as a function of the rate of cooling on primary melt-crystallization. The data serve for illustration of the effect of the condition non-isothermal crystallization on the mechanical behavior. Modulus data were measured by DMA (squares, stars) and by tensile stress–strain testing (diamond symbols, crosses). The data collected by different methods agree, which indicates negligible instrumental and analytical errors. The filled and open symbols represent data which were obtained on samples with lamellar crystals and nodular crystals, respectively, and the cross-filled symbols show the effect of annealing for preparations, which initially were melt-crystallized at rates of cooling of 0.1 and 750 K s^{-1}. The stars and cross symbols indicate presence of both lamellae and nodules within the sample. Symbol designation is identical for the yield-strength data. The classification of the crystallization regimes, introduced in Fig. 1, is indicated in the top graph.

First of all, it can be recognized that the dependencies of the modulus of elasticity and the yield strength on the conditions of crystallization are identical. The modulus of elasticity and the yield strength decrease with increasing rate of cooling on non-isothermal melt-crystallization between 10^{-1} and 10^{2} K s^{-1}, and adopt a constant, rather low value if the cooling rate is increased further. Conventional crystallization, that is, crystallization at rather low supercooling occurred on cooling at rates between 10^{-1} and 10^{2} K s^{-1}, and led to samples of relatively high modulus of elasticity and yield strength. The observed decrease with increasing rate of cooling, which is equivalent to a decrease of the crystallization temperature, is likely due to superimposed effects of a lowering of the crystallinity, thickness of lamellae, and spherulite size. If the cooling rate exceeds 10^{2} K s^{-1}, then mesophase formation is observed, apparently being independent on the cooling rate. Recent quantitative measurements of the kinetics of mesophase formation as a function of temperature [12] showed that the maximum liquid – mesophase transformation rate is close to ambient temperature. In other words, aging of quenched samples, regardless the exact rate of cooling always leads to identical structure, that is, amount of mesophase, if samples are aged at ambient temperature until a stationary structural state is achieved. Consequently, properties are then identical.

The data of Fig. 3 furthermore provide quantitative information about the change of the mechanical characteristics of differently crystallized iPP as a result of annealing at elevated temperature, though qualitatively the influence of annealing

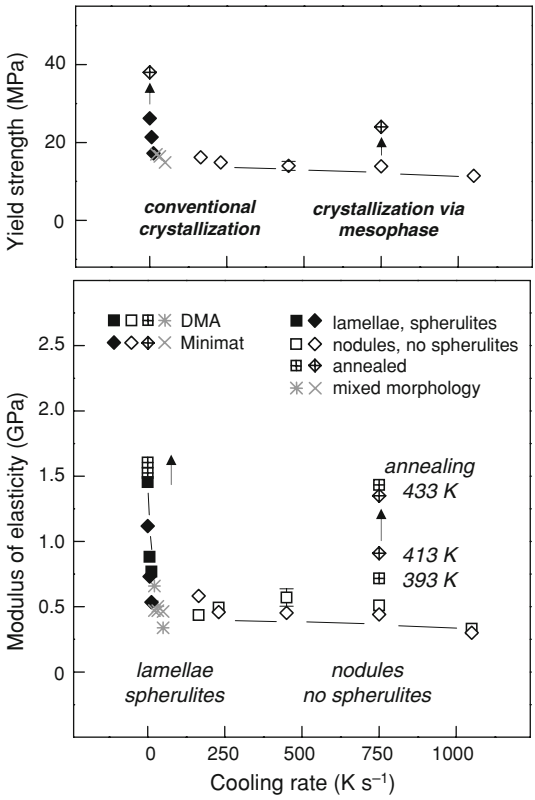

Fig. 3 Modulus of elasticity (*bottom*) and yield strength of iPP (*top*) as a function of the cooling rate on non-isothermal melt-crystallization

has already been demonstrated with the tensile stress–strain curves of Fig. 2. Annealing at elevated temperature causes a distinct increase of the modulus of elasticity and yield strength in both cases, conventionally crystallized iPP and via the mesophase-crystallized iPP. Remarkably, at least in case of the modulus of elasticity, annealing at 433 K led to almost identical values for initially slowly cooled and quenched specimens. In detail, the modulus of elasticity increased from 0.5 to 1.45 GPa due to annealing at 433 K in case of the sample which initially was crystallized by cooling at a rate of 750 K s^{-1} and subsequently aged at ambient temperature. The value of 1.45 GPa is almost identical to that obtained on the sample which initially was melt-crystallized at 0.1 K s^{-1}. Note again that the structures at both the nanometer scale, that is, the crystal morphology, and at the micrometer scale, that is, the higher-order superstructure, are qualitatively different in these samples due to the different initial crystallization step. The only identical structural parameter is the mass fraction of monoclinic crystal phase, which therefore must be considered as primary factor controlling the modulus of elasticity and the yield strength.

In Fig. 4 is plotted the modulus of elasticity of iPP of different history of crystallization as a function of the mass fraction of monoclinic crystals or mesophase to demonstrate the superior effect of the crystallinity. Squares and diamond symbols represent data obtained on iPP containing lamellae within

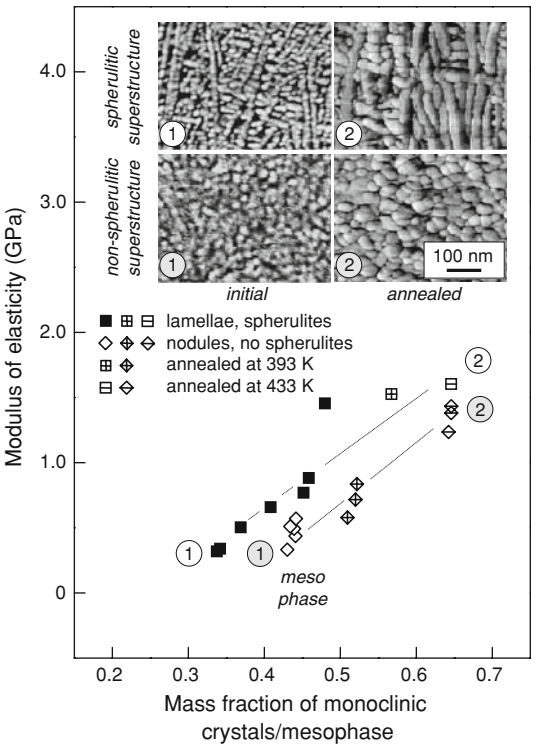

Fig. 4 Modulus of elasticity of iPP of different history of crystallization and therefore structure as a function of mass fraction of monoclinic crystals or mesophase. The *top* and *bottom* two AFM micrographs show lamellae and nodules, as were obtained by conventional crystallization and crystallization via the mesophase, respectively, before (*left*) and after annealing (*right*). AFM images were adapted with permission from Zia et al. [34], Copyright 2008 American Chemical Society

spherulites and nodules in a non-spherulitic superstructure, respectively. Symbols containing a cross or a horizontal bar indicate that samples were annealed at 393 or 433 K, respectively. In addition, at the top of Fig. 4 are shown AFM micrographs of selected samples, which either were conventionally crystallized (top images) or crystallized via the mesophase (bottom images), before and after annealing [34]. The circled numbers provide a direct link between the structure and the modulus of elasticity. First of all, the data of Fig. 4 support the general expectation of an increase of the modulus of elasticity with increasing crystallinity, with the expectation based on the commonly applied Reuss or Voigt approximation of superposition of properties of different phases [35]. Furthermore, we are able to clearly identify an effect of the crystal morphology and/or superstructure on the modulus of elasticity. Non-spherulitic samples which contain non-lamellar crystals exhibit slightly lower values of the modulus of elasticity than samples which contain cross-hatched lamellar crystals in a spherulitic superstructure, despite identical fraction of crystals.

Yield strength, σ_y, and modulus of elasticity, E, of the samples of this study are linearly correlated to each other and fit a single curve independent of the history of crystallization, and, therefore, structure. We observed a relation of $\sigma_y = 0.0225 \times E$, with the observed proportionality constant of 0.0225 being close to the value of 0.025 reported in the literature as a universal average obtained by analysis of a larger number of polymers [36, 37]. We do not intend in this study to discuss the relationship between

yield strength and modulus of elasticity from physics point of view, rather intend to show that the experimental observations of this study are reliable and worthwhile to correlate to the structure. As such, we plotted in Fig. 5, the yield strength as a function of the mass fraction of ordered phase. This plot leads to identical conclusions regarding the effects of crystallinity and crystal morphology/superstructure on the tensile stress–strain behavior as were drawn from the data of Fig. 4. The yield strength increases with increasing crystalline fraction and is for samples which contain non-lamellar crystals in a non-spherulitic superstructure slightly but reproducible lower than in case of samples containing lamellae and spherulites.

The influence of the crystal morphology and superstructure of semicrystalline polymers on both the modulus of elasticity and the yield strength is not well explored yet. This must mainly be attributed to the fact that these parameters of structure in most polymers cannot be varied independent of the crystallinity. This is true on attempting a variation of the physical structure by both changing the conditions of crystallization as well as chemical modification/random copolymerization. As such, there are only a few reports available in which an effect of the crystal morphology and superstructure on the yield strength is reported [38, 39]. In short, in case of linear low density polyethylene with butyl branches of 30% crystallinity, it was found that the yield strength of quenched preparations is lower than in slowly cooled specimen [38]. Quenching and slow cooling both resulted in formation of lamellae of identical thickness. However, the lateral extension of lamellae was lower after quenching, being, therefore, considered as an additional factor besides the crystallinity controlling the yield strength [38]. Similarly, in case of the iPP samples of this study, the lateral dimension of crystals is lower when crystallization occurred via the mesophase, leading to lower values of the yield strength and Young's modulus. Note that the crystal thickness of the iPP samples, which were crystallized according to the different routes shown in Fig. 1, at least

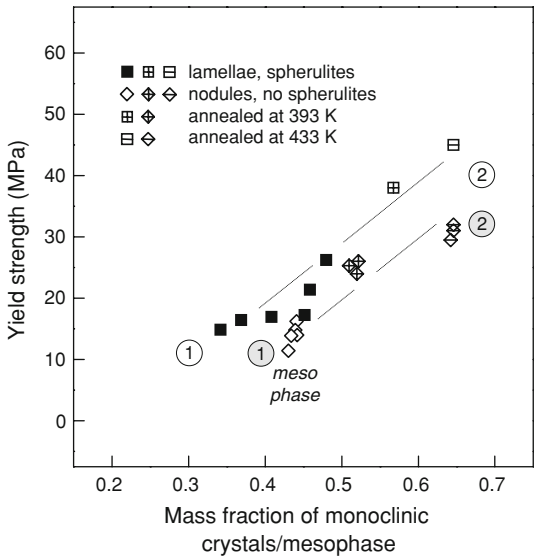

Fig. 5 Yield strength of iPP of different history of crystallization and, therefore, structure as a function of mass fraction of monoclinic crystals or mesophase. The circled numbers provide the link to the AFM micrographs shown in the upper part of Fig. 4

after annealing, probably is close to identical, since it is proven that the melting temperatures are indifferent [5].

In situ observation of deformation by atomic force microscopy (AFM)

In Fig. 6 are shown AFM height mode images of iPP films prepared by rapid cooling of the liquid at a rate of 750 K s^{-1}, before annealing (top images) and after annealing at 433 K (bottom images). The left micrographs show the structure before tensile deformation. It can be seen that after rapid cooling the specimen consists of nodules of a size of about 15–20 nm which are embedded in an amorphous matrix. From X-ray measurements, it is known that these nodules are of mesomorphic structure. Annealing resulted in an increase of the size of nodules to about 35–40 nm, and a transition into a monoclinic structure.

Tensile deformation was followed by collection of images at stepwise increasing strain until failure. During image collection, the sample was kept at constant strain. The direction of loading is indicated by the arrows in Fig. 6. It can be seen that in both cases of non-annealed (top images) and annealed samples (bottom images), the initial structure of randomly distributed nodules is transferred into a structure of parallel aligned fibrils with a lateral dimension which is similar as the initial size of nodules. The process of fibril formation seems to proceed via prior alignment of nodules which in particular can be seen in the images obtained on the non-annealed sample. Although fibrils of the non-annealed sample appear rather homogenous, close inspection still reveals internal heterogeneity, in spite of contrast being low. Qualitatively, structure reformation during tensile loading of the non-annealed and annealed specimens is similar, and differences concern only the percentage of maximum deformation before fracture. Naturally, it is expected that the sequence of

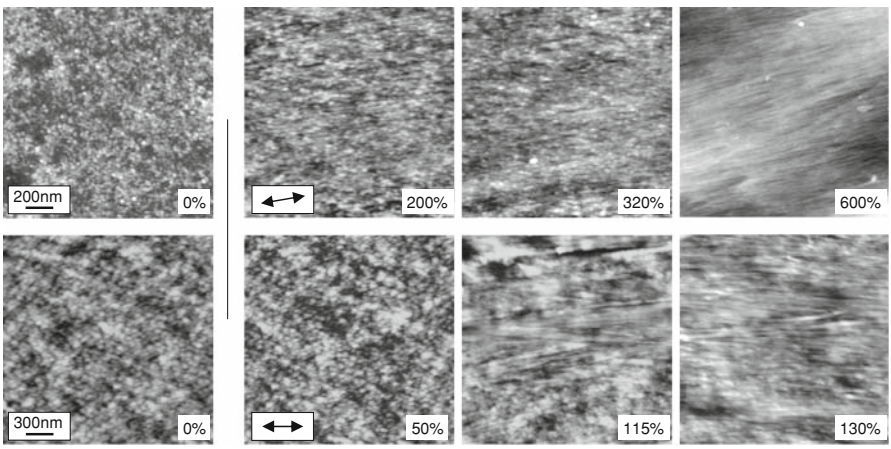

Fig. 6 In situ AFM observation of deformation of iPP films crystallized via the mesophase. Images of the *top row* show the deformation of non-annealed mesomorphic iPP, obtained by rapid cooling at a rate of 750 K s^{-1}, and the images of the *bottom row* show the deformation of a sample which additionally was annealed at 433 K. The direction of loading is indicated with the *arrows*

nodule alignment and dissolution are different in the two selected preparations which, however, was not traced/quantified since the strain increment was too large. Nonetheless, the data of Fig. 6 illustrate that tensile loading of iPP which was prepared by crystallization via the mesophase reveals ductile behavior based on plastic deformation of the ordered phase, regardless of the crystallinity and/or their internal structure and size, confirming the nature of the corresponding stress–strain diagrams shown in Fig. 2.

In contrast, analysis of the structure of a deformed sample of conventionally crystallized iPP clearly proves absence of plastic crystal deformation. In Fig. 7 is shown an AFM micrograph obtained on iPP, initially crystallized by slow cooling at a rate of 0.1 K s^{-1}, and subsequently deformed until break. The image was taken at a location close to the fracture site, with the direction of prior loading indicated by the arrow. The micrograph clearly reveals the initial structure of cross-hatched lamellae which is typical for non-nucleated iPP crystallized at low supercooling. The radial alignment/symmetry is an unambiguous indication of a spherulitic superstructure, which, however, was independently proven by polarizing optical microscopy in a companion study of the optical transparency [4]. Importantly, the AFM image of Fig. 7 proves the absence of any plastic crystal deformation as a result of tensile loading, and the presence of intra-spherulitic cracks almost perpendicular to the direction of the external normal stress. Hardly any indication of crystal reorientation and slip is observed, confirming the macroscopically observed brittle behavior, presented in Fig. 2.

Final discussion and conclusions

Primary goal of the present study was to establish a relation between the condition of crystallization, the structure at the nanometer and micrometer scale, and the mechanical performance of iPP as is assessed by tensile loading at ambient temperature and low strain rate. Samples were prepared using qualitatively different pathways of crystallization which are schematically presented in Fig. 1. Conventional melt-crystallization at low supercooling resulted in formation of cross-hatched monoclinic lamellae and a spherulitic superstructure, with the crystallinity, thickness of lamellae, and size of spherulites adjustable by the crystallization temperature, or temperature of subsequent annealing. Crystallization via formation of a mesophase and their reorganization by annealing at elevated temperature, in contrast, led to qualitatively different structures at both the nanometer and micrometer length scales. Crystals are of non-lamellar, nearly isometric habit, and spherulites are not formed. Similarly, the crystallinity and size of these nodular crystals were controlled within wide limits. The exact link between the condition of crystallization and the structure of iPP at the various length scales was the subject of prior studies [4–6, 40], and is explained in this study only for purpose of understanding their relation to the mechanical characteristics.

The tensile deformation at large strain was characterized by standard tensile stress–strain testing. These tests revealed brittle behavior for specimens which were conventionally crystallized, and ductile behavior for specimens which were

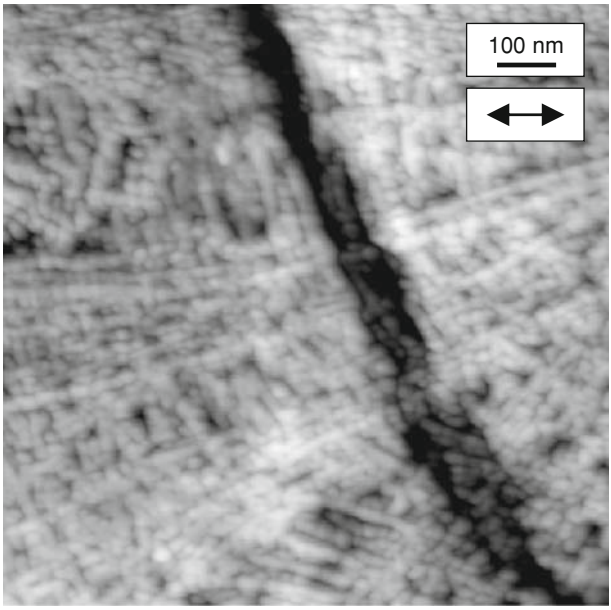

Fig. 7 AFM micrograph of the structure of conventionally crystallized iPP after tensile deformation and brittle fracture. The direction of prior loading is indicated by the *arrow*

crystallized via formation of a mesophase. The different large-strain deformation behavior is almost independent of the crystallinity, which unambiguously leads to the conclusion that the ductility is controlled by the crystal shape, the superstructure, and/or the linkage between phases. Non-lamellar crystals, which are connected by tie molecules, originally introduced by the initial crystallization step, support ductile deformation.

Tensile loading of semicrystalline polymers first leads to deformation of amorphous structure, since the average modulus of elasticity of the amorphous phase is distinctly lower than that of the crystalline phase. Stress is transferred to crystals by tie molecules which then contribute to deformation by rotation and slip. We may speculate that the brittle and ductile response of specimens with lamellar and nodular crystals, respectively, is due to different transfers of stress between the amorphous and crystalline phases. It is expected that in conventionally crystallized preparations, containing lamellae with rather perfect regular fold surfaces, the number of tie molecules is lower than in samples with nodular crystals which initially were formed at extremely high supercooling. Crystallization at high supercooling typically occurs by simultaneous formation of a large number of secondary nuclei at the crystal growth front and with that to structured surfaces. Consequently, the number of molecule segments traversing between phases is increased. Limited stress transfer between phases, that is, brittle deformation in conventionally crystallized preparations is supported by the AFM image of Fig. 7. Failure occurred intra-spherulitic without prior destruction of spherulites, rotation, or even plastic deformation of crystals. In contrast, in specimens crystallized via the

mesophase, randomly oriented nodules are embedded in the amorphous phase and likely are connected by a larger number of tie molecules. Tensile loading first leads to deformation/alignment of amorphous chain segments. Tie molecules transmit stress to nodules which are interconnected, causing their orientation and alignment into the draw direction. As a result, chain segments within nodules and amorphous regions are oriented parallel to the direction of loading. All these processes were identified by in situ AFM observation of the deformation shown in Fig. 6. We were not able to detect slip or disintegration of nodular crystals by AFM in this present study, likely due to experimental reasons. As such, we do not exclude crystal slip as major mechanism of structure reformation/fibrillation on axial loading in these samples. The observation of a distinct yield point in the stress–strain diagram even supports such processes.

The tensile deformation at small strain was characterized by the modulus of elasticity and the yield strength. These quantities increase as expected with increasing crystallinity since the modulus/strength of the crystalline phase is distinctly larger than that of the amorphous phase. The modulus of elasticity of the amorphous phase probably is of the order of only 10^0–10^2 MPa, since the temperature of testing is around or slightly higher than the glass transition temperature [34]. Note that the modulus of amorphous structure in a semicrystalline environment may increase with increasing crystallinity [41]; however, it probably does not exceed 10^2 MPa, even in samples of high crystallinity. The spatially averaged modulus of the crystalline phase, in contrast, is about 10^3–10^4 MPa, that is, it is 2–3 magnitudes of order higher than that of the amorphous phase. The modulus of elasticity of semicrystalline composite-like specimens is then estimated by using mixing rules, with the upper and lower bounds given by the well-known Voigt uniform strain and Reuss uniform stress approximations, respectively. These simple models do not take into account, e.g., the elastic anisotropy of crystals, related to largely different bond energies in chain and cross-chain direction, or the geometry/habit of crystals. Further developments/refinements of models [42–45] consider these important structural features of semicrystalline polymers, and lead to the prediction that an increase of the lateral dimension of crystals toward a lamellar geometry is connected with an increase of the lower bound approximation. Qualitatively, this fits our experimental observation shown in Fig. 4 since in case of samples with lamellae the modulus of elasticity is indeed higher than in preparations with non-lamellar crystals but identical crystallinity. Since experimental data of this kind are extremely rare, due to difficulty of preparation of highly crystalline specimens containing crystals of non-lamellar habit, we see the value of this study also in the increase of the experimental data base for further development of models for prediction of mechanical properties of polymers.

Finally, we conclude from the results of this study that crystallization of iPP via the mesophase may result in favorable combination of optical and mechanical properties which cannot be realized by conventional crystallization. Crystallization via the mesophase allows the preparation of optically highly transparent films as is demonstrated with the macrographs in Fig. 8. Complete absence of spherulites, which even is not achieved on application of optical clarifiers, increases the forward light transmission of 100 μm thick films to values of 90–95% [4], as is shown with

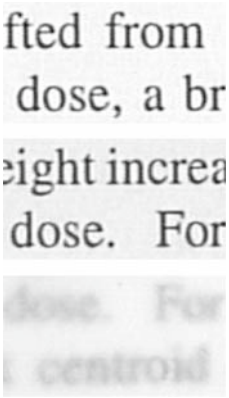

Fig. 8 Macrographs of iPP films of 100 μm thickness, crystallized via the mesophase (*center*), or conventionally crystallized (*bottom*). Polymer films were placed on the top on a text page for demonstration of different see-through clarity. Forward light transmission was measured by UV/VIS spectroscopy with the percentage values valid for a wavelength of 500 nm. Crystallization via the mesophase yields transparent films of high ductility, and high modulus of elasticity

the center image. Simultaneously, the modulus of elasticity and the yield strength are at almost identical level as in conventionally crystallized iPP, and the ductility/toughness even considerably increased. In contrast, as is illustrated through the bottom image in Fig. 8, the presence of spherulites and lamellae in conventionally crystallized iPP films reduces the forward light transmission to values lower than 50%, and causes brittle response on mechanical loading, respectively.

Acknowledgment Financial support by the Deutsche Forschungsgemeinschaft (DFG) and the ministry of culture of Saxony-Anhalt (Germany) is greatly acknowledged.

References

1. Pasquini N, Addeo A (2005) Polypropylene handbook. Hanser, Munich
2. Holliday L, White JW (1971) Stiffness of polymers in relation to their structure. Pure Appl Chem 26:545–582
3. Pritchard R (1964) The transparency of crystalline polymers. SPE Trans 4:66–71
4. Mileva D, Androsch R, Radusch HJ (2009) Effect of structure on light transmission in isotactic polypropylene and random propylene-1-butene copolymers. Polym Bull 62:561–571
5. Zia Q, Androsch R, Radusch HJ, Piccarolo S (2006) Morphology, reorganization and stability of mesomorphic nanocrystals in isotactic polypropylene. Polymer 47:8163–8172
6. Zia Q, Radusch HJ, Androsch R (2007) Direct analysis of annealing of nodular crystals in isotactic polypropylene by atomic force microscopy, and its correlation with calorimetric data. Polymer 48:3504–3511
7. Natta G, Corradini P (1960) Structure and properties of isotactic polypropylene. Nuovo Cimento 15(Suppl 1):40–51
8. Addink EJ, Beintema J (1961) Polymorphism of crystalline polypropylene. Polymer 2:185–193
9. Gezovich DM, Geil PH (1968) Morphology of quenched polypropylene. Polym Eng Sci 8:202–207
10. Hsu CC, Geil PH, Miyaji H, Asai K (1986) Structure and properties of polypropylene crystallized from the glassy state. J Polym Sci B Polym Phys 24:2379–2401
11. Piccarolo S (1992) Morphological changes in isotactic polypropylene as a function of cooling rate. J Macromol Sci B 31:501–511

12. Silvestre C, Cimmino S, Duraccio D, Schick C (2007) Isothermal crystallization of isotactic poly(propylene) studied by superfast calorimetry. Macromol Rapid Commun 28:875–881
13. Zannetti R, Celotti G, Fichera A, Francesconi R (1969) The structural effects of annealing time and temperature on the paracrystal–crystal transition in isotactic polypropylene. Die Makromol Chem 128:137–142
14. Androsch R (2008) In situ atomic force microscopy of the mesomorphic–monoclinic phase transition in isotactic polypropylene. Macromolecules 41:533–535
15. Natale R, Russo R, Vittoria V (1992) Crystallinity of isotactic polypropylene films annealed from the quenched state. J Mater Sci 27:4350–4354
16. Peterlin A (1971) Molecular model of drawing polyethylene and polypropylene. J Mater Sci 6:490–508
17. Bowden PB, Young RJ (1974) Deformation mechanisms in crystalline polymers. J Mater Sci 9:2034–2051
18. Lin L, Argon AS (1994) Structure and plastic deformation of polyethylene. J Mater Sci 29:294–323
19. Aboulfaraj M, G'Sell C, Ulrich B, Dahoun A (1995) In situ observation of the plastic deformation of polypropylene spherulites under uniaxial tension and simple shear in the scanning electron microscope. Polymer 36:731–742
20. Pang Y, Dong X, Liu K, Han CC, Chen E, Wang D (2008) Ductile–brittle transition controlled by isothermal crystallization of isotactic polypropylene and its blend with poly(ethylene-*co*-octene). Polymer 49:4259–4270
21. Lotz B, Wittmann JC (1986) The molecular origin of lamellar branching in the α (monoclinic) form of isotactic polypropylene. J Polym Sci B Polym Phys 24:1541–1558
22. Karger-Kocsis J, Varga J (1996) Effects of β–α transformation on the static and dynamic tensile behavior of isotactic polypropylene. J Appl Polym Sci 62:291–300
23. Kotek J, Raab M, Baldrian J, Grellmann W (2002) The effect of specific β-nucleation on morphology and mechanical behavior of isotactic polypropylene. J Appl Polym Sci 85:1174–1184
24. Gezovich DM, Geil PH (1968) Deformation and aging of quenched polypropylene. Polym Eng Sci 8:210–215
25. Seguela R, Staniek E, Escaig B, Fillon B (1999) Plastic deformation of polypropylene in relation to crystalline structure. J Appl Polym Sci 71:1873–1885
26. De Candia F, Russo R, Vittoria V (1987) Mechanical behavior of quenched isotactic polypropylene crystallized by thermal and solvent treatments. J Appl Polym Sci 34:689–701
27. Ferrer-Balas D, Maspoch MLL, Martinez AB, Santana OO (2001) Influence of annealing on the microstructural, tensile and fracture properties of polypropylene films. Polymer 42:1697–1705
28. Way JL, Atkinson JR, Nutting J (1974) The effect of spherulite size on the fracture morphology of polypropylene. J Mater Sci 9:293–299
29. Remaly LS, Schultz JM (1970) Time-dependent effect of spherulite size on the tensile behavior of polypropylene. J Appl Polym Sci 14:1871–1877
30. Koike Y, Cakmak M (2004) Atomic force microscopy observations on the structure development during uniaxial stretching of PP from partially molten state: effect of isotacticity. Macromolecules 37:2117–2181
31. Crämer K, Schneider M, Mülhaupt R, Cantow HJ, Magonov SN (1994) Scanning force microscopy of oriented iso- and syndiotactic polypropylene films. Polym Bull 32:637–644
32. Brucato V, Piccarolo S, La Carrubba V (2002) An experimental methodology to study polymer crystallization under processing conditions. The influence of high cooling rates. Chem Eng Sci 57:4129–4143
33. De Santis F, Adamovsky S, Titomanlio G, Schick C (2006) Scanning nanocalorimetry at high cooling rate of isotactic polypropylene. Macromolecules 39:2562–2567
34. Zia Q, Mileva D, Androsch R (2008) Rigid amorphous fraction in isotactic polypropylene. Macromolecules 41:8095–8102
35. McGee S, McCullough RL (1981) Combining rules for predicting the thermoelastic properties of particulate filled polymers, polyblends, and foams. Polym Compos 2:149–161
36. Seitz JT (1993) The estimation of mechanical properties of polymers from molecular structure. J Appl Polym Sci 49:1331–1351
37. Rowe RC, Roberts RJ (1995) Interrelationships between the yield stress, tensile fracture strength and Young's modulus of elasticity of films prepared from cellulose ethers and esters. J Mater Sci Lett 14:420–421

38. Graham JT, Alamo RG, Mandelkern L (1997) The effect of molecular weight and crystallite structure on yielding in ethylene copolymers. J Polym Sci B Polym Phys 35:213–223
39. Androsch R, Stribeck N, Lüpke T, Funari SS (2002) Investigation of the deformation of homogeneous poly(ethylene-co-1-octene) by wide- and small-angle X-ray scattering using synchrotron radiation. J Polym Sci B Polym Phys 40:1919–1930
40. Zia Q, Androsch R, Radusch HJ, Ingolič E (2008) Crystal morphology of rapidly cooled isotactic polypropylene: a comparative study by TEM and AFM. Polym Bull 60:791–798
41. Crist B, Fisher CJ, Howard PR (1989) Mechanical properties of model polyethylenes: tensile elastic modulus and yield stress. Macromolecules 22:1709–1718
42. Boyd RH (1983) The mechanical moduli of lamellar semicrystalline polymers. J Polym Sci B Polym Phys 21:493–504
43. Doyle MJ (2000) On the effect of crystallinity on the elastic properties of semicrystalline polyethylene. Polym Eng Sci 40:330–335
44. Halpin JC, Kardos JL (1976) Halpin-Tsai equations: a review. Polym Eng Sci 16:344–352
45. Bédoui F, Diani J, Régnier G (2004) Micromechanical modeling of elastic properties in polyolefins. Polymer 45:2433–2442